

COVER PAGE

Document downloaded by @DAEL

Sun Nov 29 16:31:22 2026
For personal use

When automatic English translation is provided, only the original document is authentic.
The EAA cannot be held responsible of any translation error

Bibliographical reference

Improved Low Frequency Room Responses by Considering Finiteness of Room Boundary Surfaces, Cheol-Ho Jeong, Acta Acustica **vol. 99** (Number 4), 2013, pp. 545-556

DOI
https://doi.org/10.3813/AAA.918634

Acta Acustica united with Acustica
Vol. 99 (2013) 545 – 556

DOI 10.3813/AAA.918634

Improved Low Frequency Room Responses by Considering Finiteness of Room Boundary Surfaces

Cheol-Ho Jeong
Acoustic Technology, Department of Electrical Engineering, Technical University of Denmark, 2800, Kongens Lyngby, Denmark. chj@elektro.dtu.dk

Summary
For room acoustic simulations, the acoustic characteristics of room boundary surfaces are typically calculated under the assumption that the surfaces are sufficiently large. In this study, a reflection coefficient for finite surfaces is suggested and its performance is assessed through case studies involving simulation of rectangular rooms using a phased beam tracing method. The suggested reflection coefficient employs the radiation impedance of a finite surface by combining the radiation impedance of an infinitely large surface and that of the finite surface backed by an infinite rigid baffle. For 28 surface impedance values that are assigned to all the boundary surfaces, the suggested reflection coefficient is found to improve low frequency responses compared to the infinite panel theory; larger improvements are found for a more disproportionate room, more absorptive surfaces, and surfaces having larger negative phase angles of the surface impedance. A larger improvement is also found for a non-uniform absorption case than for a uniform absorption setting having a similar equivalent absorption coefficient.

PACS no. 43.55.Ke, 43.55.Dt

1. Introduction

In reality, rooms have finite boundary surfaces. However, quantifying the sound absorption coefficient of a finite surface is neither easy nor straightforward, and therefore many acousticians have used sound absorption coefficients for plane waves incident onto infinitely large locally reacting surfaces, namely, the random incidence absorption coefficient using Paris' law [1]:

$$\alpha_{\text{rand}} = \int_0^{\pi/2} \left(1 - \left|\frac{\zeta\cos\theta - 1}{\zeta\cos\theta + 1}\right|^2\right) \sin(2\theta)\,\mathrm{d}\theta. \quad (1)$$

Here, ζ is the normalized surface impedance and θ is the incidence angle. The use of the random incidence absorption coefficient might be reasonable for large rooms that are made up of large surfaces and for high frequency analyses, but the accuracy of acoustic simulations of small rooms by assuming plane waves incident onto infinitely large panels is known to be degraded [2, 3].

There has been no good way of considering finiteness in calculating the absorption coefficients of room boundary surfaces. The size effect has been a crucial topic for standard measurements of sound absorption, i.e., the reverberation chamber method according to, e.g., ISO 354 [4]. Measured sound absorption coefficients vary largely with the sample size, therefore the standard recommends a minimum size of the test sample. If the absorber under test is backed by an acoustically rigid surface, a theoretical derivation by Thomasson [5] has been successfully used to estimate absorption coefficients measured in reverberation chambers, called the Sabine absorption coefficient [5, 6, 7]. The consideration of finite surfaces is quite straightforward in Thomasson's formulation by replacing the radiation impedance of $1/\cos(\theta)$ for large surfaces by the radiation impedance for a finite surface. However, Thommason's formulation cannot be directly applied to realistic room boundary surfaces, e.g., surfaces that are interconnected at right angles in rectangular rooms, because Thomasson assumed an infinitely large rigid baffle condition surrounding the absorbent sample.

This study aims to suggest a practical reflection coefficient for finite surfaces mainly for use in simulations of rectangular rooms with uniform absorption treatment at low frequencies. The suggested reflection coefficient can improve room acoustic simulations mostly at low frequencies. The key aspect of the reflection coefficient for a finite surface is a new radiation impedance that combines the radiation impedance of an infinitely large surface and that of the finite surface backed by an unbounded rigid baffle. To validate the suggested reflection coefficient, a phased beam tracing model is used as a tool [8], which can employ various reflection coefficients, and finally phased beam tracing simulations are compared with boundary element simulations to quantify simulation errors. The sug-

Received 19 November 2012,
accepted 5 May 2013.

© S. Hirzel Verlag · EAA

gested reflection coefficient is tested in two rectangular rooms for various uniformly-treated absorption cases and a realistic non-uniform distribution case.

2. Consideration of finiteness

This study is only concerned with a locally reacting rectangular absorber of dimensions of a and b (all dimensions in m in what follows). By comparing the sound pressure distributed over three boundary configurations around the sample, one can get an idea of the reflection coefficient of a finite surface.

2.1. Three configurations

Assume a finite-sized rectangular absorber having a normalized surface impedance of ζ. Imagine three configurations in Figure 1. The first configuration is the absorber surrounded by an infinitely large surface of the same material as shown in Figure 1a. The reflection coefficient that represents this configuration is the well-known reflection coefficient for oblique incidence of a plane wave into an infinitely extended locally reacting surface as

$$r_{\mathrm{inf}} = \frac{\zeta - \zeta_{\mathrm{rad,inf}}}{\zeta + \zeta_{\mathrm{rad,inf}}} = \frac{\zeta - 1/\cos\theta}{\zeta + 1/\cos\theta}. \tag{2}$$

The magnitude of the total sound pressure over the absorber in this configuration is completely uniform as $p_i(1+r_{\mathrm{inf}})$, where p_i is the incident pressure.

The second configuration is that the same finite absorber surrounded by an infinitely large rigid baffle as shown in Figure 1b. This condition is then equivalent to what Thomasson assumed in his derivation [5]. The reflection coefficient for this case is expressed as

$$r_{\mathrm{Thom}} = \frac{\zeta - \zeta_{\mathrm{rad,baffle}}(f,a,b,\theta,\varphi)}{\zeta + \zeta_{\mathrm{rad,baffle}}(f,a,b,\theta,\varphi)}. \tag{3}$$

Note that this reflection coefficient can be interpreted in a way that the radiation impedance of $1/\cos(\theta)$ for infinite surfaces is replaced by another radiation impedance for finite surfaces. Naturally $\zeta_{\mathrm{rad,baffle}}$ varies with the frequency, the dimensions of the finite surface (a and b), and two incidence angles, θ as the elevation incidence angle and φ as the azimuth incidence angle. Refer to section 2.2 for detailed information about $\zeta_{\mathrm{rad,baffle}}$. In this case the sound pressure over the surface would not be uniform, as the pressure at the boundary edges will converge to $2p_i$, whereas the pressure over the central region of the absorber is $p_i(1 + r_{\mathrm{inf}})$. Thus, the averaged sound pressure over the absorber in this configuration is higher than that in the infinitely extended absorber configuration, thus the corresponding reflection coefficient averaged over the absorber, r_{Thom}, should be larger than r_{inf}.

The third configuration is that several finite absorbers having the same acoustic characteristic are interconnected to each other at right angles, which is similar to a rectangular room with uniformly distributed absorption, but without a ceiling, as shown in Figure 1c. Due to the vertical boundary surfaces, the averaged pressure around the edges of the absorber will be higher than $p_i(1 + r_{\mathrm{inf}})$, but it would not be as high as $2p_i$, since the vertical surfaces are not acoustically rigid in most cases. If the vertical surfaces are acoustically rigid, the magnitude of the total sound pressure can be higher than $2p_i$, but such conditions are not highly likely. It is worth-mentioning that Ljunggren investigated similar configurations for sound transmission, and concluded that sound transmission of a test wall mounted by orthogonal partitions is lower than with the wall mounted in an infinite baffle [9]. Therefore the reflection coefficient for the third configuration is likely to be in-between those for the first two configurations. One may come up with an approximate reflection coefficient for the third configuration by combining the first two.

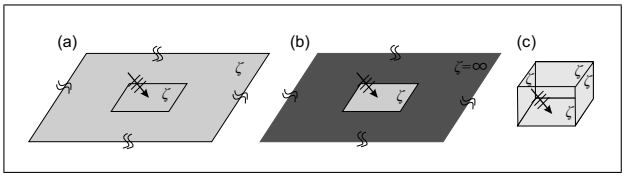


Figure 1. A finite-sized absorber with three surrounding configurations. (a) Infinitely extended absorber, (b) backed by an infinitely large rigid baffle, (c) connected to vertical finite surfaces.

For uniformly distributed absorption cases, the third configuration is more similar to the first configuration than the second, since at least the surface characteristics of the absorber and surrounding surfaces are identical. Obviously, the major difference of the second configuration from the first and third is the acoustic characteristic of the surrounding surfaces, which is always fixed to acoustically rigid. None of the first two configurations is similar to the third case in terms of the geometry of the connection; the first two configurations have horizontal connections to the surrounding surfaces, while the third one has right angle connections between the absorber and other surrounding surfaces. As the surface impedance of the absorber becomes infinity, thus totally reflective, the first two configurations become identical.

As a first attempt, the radiation impedance of the finite surface in the third configuration is assumed to be the average of the radiation impedance of the infinitely extended surface and rigidly baffled surface. Thus the reflection coefficient for the finite-sized rectangular boundary surface is expressed as

$$r_{\mathrm{fin}} = \frac{\zeta - \zeta_{\mathrm{rad,fin}}}{\zeta + \zeta_{\mathrm{rad,fin}}} = \frac{\zeta - (\zeta_{\mathrm{rad,baffle}} + 1/\cos\theta)/2}{\zeta - (\zeta_{\mathrm{rad,baffle}} + 1/\cos\theta)/2}. \tag{4}$$

The suggested reflection coefficient can potentially be problematic at grazing incidence angles, since the term $1/\cos\theta$ in equation (4) will dominate at angles, say, above 80°, which also happens with the infinite panel theory. The radiation impedance of a finite surface depends on the following factors: the shape and size of the test absorber, the angle of the incident wave, and frequency. In addition it is also influenced by the sound field inside the room, in other

Table I. Radiation impedance of a square with an edge length of e [11].

ke	0°	15°	30°	45°	60°	75°	90°
≤ 0.5	$Z_f = (ke)^2/2\pi - \mathrm{j}0.473(ke)$						
0.50	0.04 − j0.23	0.04 − j0.23	0.04 − j0.23	0.04 − j0.23	0.04 − j0.23	0.04 − j0.23	0.04 − j0.23
0.71	0.08 − j0.32	0.08 − j0.32	0.08 − j0.32	0.08 − j0.32	0.08 − j0.31	0.07 − j0.32	0.07 − j0.32
1.00	0.15 − j0.43	0.15 − j0.43	0.15 − j0.43	0.14 − j0.43	0.14 − j0.42	0.14 − j0.42	0.14 − j0.43
1.41	0.28 − j0.56	0.28 − j0.56	0.27 − j0.55	0.26 − j0.54	0.25 − j0.53	0.25 − j0.53	0.24 − j0.53
2.00	0.51 − j0.66	0.50 − j0.66	0.48 − j0.65	0.44 − j0.64	0.41 − j0.63	0.39 − j0.62	0.38 − j0.62
2.82	0.82 − j0.65	0.80 − j0.65	0.73 − j0.66	0.65 − j0.68	0.58 − j0.68	0.53 − j0.69	0.52 − j0.69
4.00	1.07 − j0.41	1.04 − j0.46	0.96 − j0.57	0.84 − j0.67	0.74 − j0.75	0.66 − j0.78	0.64 − j0.79
5.66	1.02 − j0.14	1.06 − j0.22	1.11 − j0.43	1.06 − j0.66	0.94 − j0.82	0.84 − j0.90	0.80 − j0.92
8.00	0.94 − j0.19	1.01 − j0.16	1.19 − j0.25	1.28 − j0.56	1.18 − j0.87	1.03 − j1.03	0.97 − j1.08
11.31	1.02 − j0.09	1.03 − j0.14	1.14 − j0.15	1.43 − j0.38	1.46 − j0.86	1.27 − j1.18	1.17 − j1.26
16.00	1.01 − j0.09	1.03 − j0.08	1.14 − j0.14	1.43 − j0.20	1.75 − j0.77	1.56 − j1.33	1.14 − j1.48
22.63	1.01 − j0.06	1.04 − j0.06	1.15 − j0.08	1.38 − j0.15	1.98 − j0.56	1.92 − j1.47	1.69 − j1.75
32.00	0.99 − j0.04	1.03 − j0.04	1.16 − j0.06	1.42 − j0.12	2.04 − j0.30	2.36 − j1.58	2.02 − j2.07
45.25	1.00 − j0.03	1.04 − j0.03	1.16 − j0.04	1.41 − j0.08	1.96 − j0.19	2.88 − j1.58	2.41 − j2.46
64.00	1.00 − j0.02	1.04 − j0.02	1.15 − j0.03	1.41 − j0.05	2.00 − j0.18	3.43 − j1.40	2.87 − j2.92
94.51	1.00 − j0.02	1.04 − j0.02	1.15 − j0.02	1.41 − j0.04	1.99 − j0.11	3.84 − j1.01	3.42 − j3.46
128.00	1.00 − j0.01	1.04 − j0.01	1.15 − j0.01	1.41 − j0.03	2.00 − j0.07	3.94 − j0.54	4.08 − j4.12
≥ 128	$Z_f = 1/\sqrt{\cos^2\theta + \mathrm{j}4\beta\sin\theta/(ke) + (2\beta/ke)^2},\ \beta = 0.956$						

words, by the other boundary surfaces and their distribution. Therefore it should be admitted that the suggested radiation impedance in equation (4) is indeed a simple approximation, but it is difficult to estimate the correct radiation impedance of a boundary surface in a room by purely theoretical means.

2.2. Thomasson's theory

Thomasson formulated the absorption coefficient of a surface that is backed by an infinitely large rigid baffle [5]. This assumption fits well with the standard measurement setup specified in ISO 354 [4] and ASTM C/423 [10], and therefore Thomasson's assumption has been used to account for overestimated absorption coefficients measured in reverberation chambers compared to the random incidence absorption coefficients [6, 7]. Note that this is a size correction, thus is effective only at low frequencies where the wavelength is longer than the dimensions of the test absorber. At high frequencies where the wavelength is short enough, Thomasson's formulation cannot change the results significantly.

Thomasson first derived the pressure distribution over an absorber that is backed by an infinitely large and acoustically rigid baffle. Through a variational approach, Thomasson ended up with a pressure distribution over the absorber as

$$p_a(x, y, 0) = 2p_i(x, y, 0)\frac{\zeta}{\zeta + \zeta_{\mathrm{rad,baffle}}}. \tag{5}$$

Here, p_a is the sound pressure over the absorber and p_i is the pressure of the incident wave. The radiation impedance in his original work is referred to as the field impedance [5]. The radiation impedance of a finite absorbing surface backed by an infinitely large rigid baffle is calculated by (see [5], equation 18 and [11], equation A1)

$$\zeta_{\mathrm{rad,baffle}} = \frac{-\mathrm{j}k}{S}\iint_{S_a}\iint_{S_a} G\mathrm{e}^{-\mathrm{j}k[\mu_x(x_0-x)+\mu_y(y_0-y)]}\,\mathrm{d}x\,\mathrm{d}y\,\mathrm{d}x_0\,\mathrm{d}y_0, \tag{6}$$

where k is the wavenumber, $S = \iint_{S_a}\mathrm{d}x\,\mathrm{d}y$, $\mu_x = \sin\theta\cos\phi$, $\mu_y = \sin\theta\sin\phi$, $G = -\exp(-\mathrm{j}kR)/2\pi R$, and $R = \sqrt{(x-x_0)^2 + (y-y_0)^2}$.

The radiation impedance depends mainly on the shape and size of the absorber. Assuming a weak dependence on the azimuth angle, the averaged radiation impedance as a function of the incidence angle of θ can be calculated. In [11], the radiation impedances averaged over the azimuth angle are tabulated as a function of ke and θ, in irregular steps of ke and in regular 15° intervals of θ, where e is the characteristic dimension of the surface as $2ab/(a+b)$, which are now listed in Table I. Note that $\zeta_{\mathrm{rad,baffle}}$ approaches $1/\cos\theta$ at high frequencies and for large surfaces. Rindel [12] made an approximation of the radiation impedance only for the real part of $\zeta_{\mathrm{rad,baffle}}$ as

$$\zeta_{\mathrm{rad,Rindel}}(f, \theta) = \left[\left(\cos^2\theta_i - 0.6\frac{2\pi}{ke}\right)^2 - \pi\left(0.6\frac{2\pi}{ke}\right)^2 + \left(\frac{2\pi}{(ke)^2}\right)^4\right]^{-0.25}. \tag{7}$$

Recently Brunskog modified the double surface integral in equation (6) to a double integration over two axes, enabling us to calculate the radiation impedance in Matlab using the command "dblquad" with a tolerance of 10^{-6} [13].

3. Method

Two rectangular rooms, one proportionate and one disproportionate room, were simulated by two simulations

schemes, the boundary element method and the phased beam tracing method. The boundary element simulations are considered as reference simulations, since the method is known to provide accurate results at low frequencies. 28 surface impedances were used for the proportionate room, whereas only 4 impedance values were used for the disproportionate room. A non-uniform absorption distribution was also tested in the proportionate room.

3.1. Rooms and receivers

The proportionate room has dimensions of 1.9×1.4×1 and the disproportionate room has dimensions of 5×1×1. For the proportionate room, a point source was positioned at (0.1, 0.1, 0.4) representing a talker. A total of 54 receivers were positioned with x changing from 0.15 to 1.75 with steps of 0.2, and y changing from 0.2 to 1.2 with steps of 0.2, and a fixed z of 0.3. For the disproportionate room, 36 receivers were positioned with x changing from 0.5 to 4.5 with steps of 0.5, and y changing from 0.2 to 0.8 with steps of 0.2, and a fixed z of 0.3, while the source position is located at the same point as in the proportionate room.

3.2. Boundary conditions

28 uniformly distributed absorption cases represented by the normalized surface impedance values listed in Table II were tested in the proportionate room. In terms of the random incidence absorption coefficient, they are categorized into four absorption groups of 0.2, 0.4, 0.6, and 0.8, and short-named as BC1 to BC4. For the phase angles, μ ($= \tan^{-1}(\Im m(\zeta)/\Re e(\zeta))$), of the impedance at intervals of 20°, the magnitudes of the impedances were searched and listed in Table II. For a given phase angle, there is an upper limit of the absorption coefficient, e.g., the maximum absorption coefficient for the phase angles of ±80° is 0.25, thus the random incidence absorption coefficients larger than 0.25 can have neither larger phase angles than 80° nor smaller phase angles than −80°. Finally nine surface impedance values were found for BC1, seven values for BC2 and BC3, and five values for BC4. Although real-valued surface impedance approximations have been commonly used for room acoustic simulations, it is more correct to employ complex-valued surface impedances, since most absorbers have complex-valued impedances. The phase angle is subscripted for the short names, e.g., the zero phase angle for BC1 is named as $\mathrm{BC1}_{,0}$.

In addition, a realistic non-uniform distribution in the proportionate room (with an acronym of NONU) was also tested. The ceiling, floor, and the side walls were assigned with the impedance data of [5.9, 18.0, 38.0], which corresponded to the random incidence absorption coefficients of 0.66, 0.32, and 0.17, respectively. For the disproportionate room, results only for the real-valued surface impedance values, [32.0, 13.4, 7.1, 3.9] were presented for the sake of brevity.

3.3. Simulation methods: BEM and PBTM

The boundary element method tackles acoustic problems numerically based on the discretized Helmholtz-Kirchhoff integral equation on a surface mesh [14]. An in-house boundary element model is used for comparisons. For the proportionate room, the boundary element model contains 6880 triangular elements with 3442 nodes, of which the 6 elements per wavelength condition is satisfied at 1000 Hz. The disproportionate room has 7228 elements and 3616 nodes, therefore its upper cutoff frequency is about 700 Hz. For the two rooms, the linear shape function and seven Gaussian points were used. The boundary element simulations are regarded as the reference simulations.

Table II. The magnitudes of the impedance values, $|\zeta|$, for the given phase angles, μ. $\zeta = |\zeta| \exp(\mathrm{j}\mu)$.

	0°	±20°	±40°	±60°	±80°	α_{rand}
BC1	32.0	30.0	24.3	15.5	4.1	0.2
BC2	13.4	12.5	10.0	5.9	-	0.4
BC3	7.1	6.6	5.1	2.3	-	0.6
BC4	3.9	3.5	2.2	-	-	0.8

The phased beam tracing method is a variant of the geometrical acoustics models, which retains phase information in order to account for wave phenomena, particularly interference. Inclusion of phase is two-folds: phase shift on reflection and propagation phase. The former phase requires complex-valued surface impedances. The latter phase is simply implemented based on the travelling distance from the source to receiver, d_{tavel}, and taking into account a term, $\exp(-\mathrm{j}kd_{\mathrm{tavel}})$, in calculation of sound pressures, where j is the imaginary unit, and k is the wavenumber. This phased geometrical acoustics method has been a useful tool for investigation of different reflection modeling and various boundary conditions, e.g., plane wave vs. spherical wave reflection modeling [2], comparing local and bulk reaction [15, 16], and various impedance and absorption boundary conditions [3, 17].

PBTM used in this study is based on the triangular beam tracing algorithm by Lewers [18], but extended to include phase. The tracing algorithm consists of source generation, surface-geometry definition, traces of beams, and receiver detection. Source division is based on an icosahedron, which makes the beam cross section an equilateral triangle. Then, all edges of the equilateral triangles of the icosahedron are divided into p equal lengths, resulting in a polygon with $20p^2$ triangular faces. For each point receiver, the source is rotated so that a triangle faces toward the receiver in order not to miss the direct sound. Room boundary surfaces should be planar, which are mathematically modeled as $A_i x + B_i y + C_i z + D_i = 0$. A trajectory of a beam is scanned by a combined process of determining the nearest plane, finding the new image source, and calculating the reflected vector. A beam is defined by a central axis and three boundary planes, each plane forming a side of the beam. Beams do not fragment on reflection and the direction after reflection is determined entirely by its central axis. Once the trajectory of the beam is identified, the possibility that a point receiver is surrounded by the

beam boundary planes is tested using the normal vectors of the boundary walls. Following a positive receiver detection test, the complex pressure for the beam undergoing the reflection path is calculated and finally the transfer function is constructed. Only specular reflections are counted.

Assuming a point source emitting spherical waves, the free-space Green's function [19], $A\exp(-\mathrm{j}kr)/r$, is a basis to calculate the transfer function at an observation point, where r is the distance from the source to the observation point and A is an arbitrary constant. For all simulations in this study, A is assumed to be unity, therefore producing 1 Pa at 1 m from the source in a free-field condition. The same assumption is used for BEM simulations for direct comparisons of the simulation results. For each reflection, a reflection coefficient is multiplied to the free-space Green's function. For the given impedance boundary conditions, the plane wave reflection coefficients in equations (2)–(4) are computed and multiplied to the corresponding incident pressures.

The current beam tracing model cannot account for diffraction phenomena and diffuse reflection, but it probably does not harm the calculations of sound pressures in empty rectangular rooms. For all the PBTM simulations, 8000 beams were emitted from the source, and they were traced up to the 100th reflection order. The reason for the large number of beams is due to the fact that PBTM used does not incorporate a beam-splitting algorithm. In addition, a sufficient number of late reflections should be calculated, therefore each beam was traced up to the 100th reflection order. For BC1, the average propagation distance for the 100th reflection order is 97 m, corresponding to a sufficient decay range of 45 dB. For the other boundary conditions, the decay ranges are even larger, as the reverberation times become shorter with increasing absorption.

3.4. Reflection coefficients used

The reflection coefficients in equations (2)–(4) were used for PBTM simulations, and then compared with BEM calculations. The radiation impedance for finite surfaces is assumed to be weakly dependent of the azimuth angle, and therefore averaged impedance values over the azimuth angles are calculated. In this way the radiation impedance is only a function of ke and the incidence angle, θ.

The finite-sized reflection coefficient in equation (4) was calculated in two ways. First, the radiation impedance values for a square shaped absorber were calculated for predefined sets of ke and elevation angles (θ), since the calculation of the radiation impedance for finite surfaces is computationally heavy, thus it is difficult to calculate the radiation impedance values for, say, millions of reflections in practice. The incidence angle set ranged from 0° to 90° at 5° intervals. The ke values were decided in logarithmic steps from 0.5 to 181. Then a matrix of the radiation impedance data having a size of 18×19 was computed. Note the calculation of such a matrix took one day on a PC with a quad core CPU of 3.07 GHz and a RAM of 6 GB. The precalculated radiation impedance values were used for all the reflections. For each reflection, the correct ke and θ were searched and approximated to the closest values of ke and θ in the pre-defined set, and then the pre-calculated radiation impedance for the approximated ke and θ value was used as the radiation impedance of the particular reflection. One may also use some interpolation techniques for more accurate results, which was not tried in the study. To speed up the calculation more, the reflection coefficients within 1/1 octave bands were assumed to be constant, thus the reflection coefficients were computed only at the center frequencies of the octave bands centered from 31.5 Hz to 1 kHz. Note that although the radiation impedance indeed changed with the aspect ratio of the rectangular surface, rectangular boundary surfaces were assumed to be squares, thus the radiation impedance for a square having the same characteristic dimension of e as the rectangle was computed and used for all the room surfaces. This reflection coefficient is named as $r_{\mathrm{fin,sq}}$.

Second, $r_{\mathrm{fin,Rindel}}$ is calculated by replacing $\zeta_{\mathrm{rad,baffle}}$ in equation (4) by Rindel's approximation in equation (7). Since it does not incorporate the double surface integral, the calculation is much faster. However, this reflection coefficient omits the imaginary part, thus it can be less accurate than $r_{\mathrm{fin,sq}}$.

3.5. Error measures

Transfer functions were calculated using PBTM and BEM in different frequency ranges for the two rooms: from 70 Hz to 900 Hz at 2 Hz intervals for the proportionate room, and from 20 Hz to 710 Hz at 2 Hz intervals for the disproportionate room, since their first axial modes are located at around 90 Hz and 34 Hz, respectively. From the calculated transfer functions, 1/3 octave band levels re. 1 Pa were computed, and named as $SPL_{\mathrm{PBTM,oct}}$ and $SPL_{\mathrm{BEM,oct}}$. Then the simulation error is defined as

$$e(f_c) = \left| SPL_{\mathrm{PBTM,oct}}(f_c) - SPL_{\mathrm{BEM,oct}}(f_c) \right|, \quad \text{(dB)} \quad (8)$$

where f_c means the center frequencies of the 1/3 octave bands from 80 Hz to 800 Hz for the proportionate room, and the center frequencies of the 1/3 octave bands from 31.5 Hz to 630 Hz for the disproportionate room due to the cutoff frequency of the boundary element simulation.

4. Results

4.1. Uniform absorption in the proportionate room

In Figures 2 to 5, the errors for the uniform boundary conditions are shown; the symbols in the figures indicate mean values, and the error bars show 95% confidence intervals. For BC1, the errors using the suggested reflection coefficient are improved at low frequencies as shown in Figure 2. The improvement depends on the phase angle of the impedance; generally larger improvements are found for the negative phase angles than the positive phase angles. The improvements for $\mathrm{BC1}_{,40}$ and $\mathrm{BC1}_{,60}$ are found to be insignificant. For the largest phase angles, ±80°, the largest improvements are found. Table III lists the mean

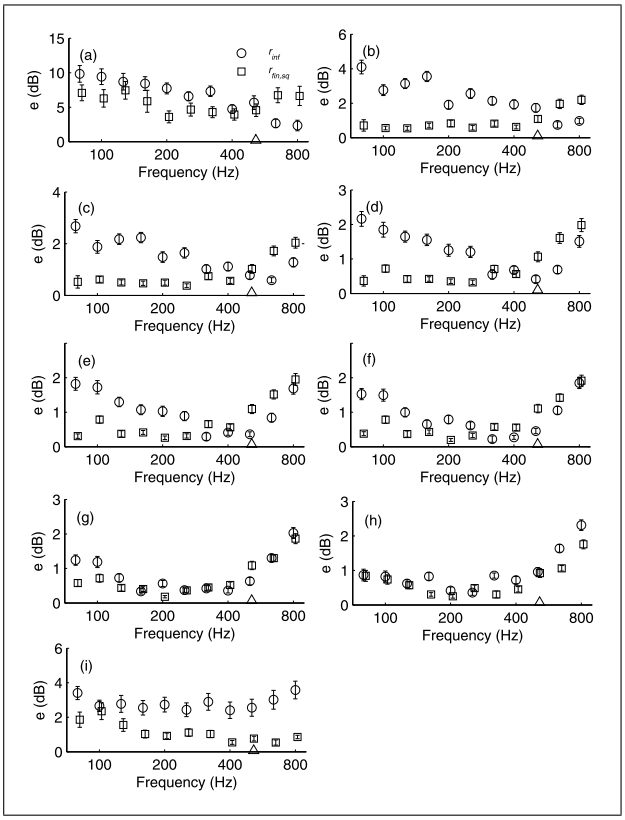


Figure 2. Errors averaged over the receiver positions as a function of frequency in the proportionate room for BC1. The error bars indicate 95% confidence intervals and Δ indicates the Schroeder frequency. (a) -80°; (b) -60°; (c) -40°; (d) -20°; (e) 0°; (f) 20°; (g) 40°; (h) 60°; (i) 80°.

and maximum reduction in the error using $r_{\mathrm{fin,sq}}$, and the highest frequency until which the suggested reflection coefficient performs better than the infinite panel theory, named as the limiting frequency, f_{lim}. Then, the ratio of f_{lim} to the Schroeder frequency, f_{Sch}, is calculated. This ratio, $f_{\mathrm{lim}}/f_{\mathrm{Sch}}$, increases as the magnitude of the phase angle increases, with exceptions of $BC1_{,40}$ and $BC1_{,60}$. $\overline{\Delta e}$ denotes the average improvement of e using $r_{\mathrm{fin,sq}}$ compared to the infinite panel theory for the entire frequency range, i.e., from 80 Hz to 800 Hz, and Δe_{max} is the maximum reduction in the error. In most cases, the maximum error reductions are achieved in the 1/3 octave band centered at 80 Hz, where the first axial mode occurs, indicating that the peak level at the first resonance frequency using $r_{\mathrm{fin,sq}}$ is more accurately predicted than using r_{inf}.

As Figure 3 and Table IV show, large improvements for BC2 at low frequencies are also found. Again similar trends to BC1 are observed; as the phase angle increases, the improvement becomes larger, and the ratio, $f_{\mathrm{lim}}/f_{\mathrm{Sch}}$ becomes higher. The improvements for the negative phase angles are clearly larger. Similar conclusions for BC3 and BC4 can be drawn from Figures 4 and 5, and Tables V and VI. Particularly for BC4, the suggested reflection coefficient outperforms the infinite panel theory regardless of the phase angles and the frequency bands tested. In all cases, the error curves become more flat by the enhanced accuracy at low frequencies. In general, the 95% confidence intervals are also reduced with $r_{\mathrm{fin,sq}}$, implying that the seat-to-seat variations are reduced.

The limiting frequency ratio, $f_{\mathrm{lim}}/f_{\mathrm{Sch}}$, increases as the surface impedance decreases; just for the zero phase angle cases, $f_{\mathrm{lim}}/f_{\mathrm{Sch}}$ changes from 0.5 to 3.1, as the absorption coefficient increases from 0.2 to 0.8, which indicates that the suggested reflection coefficient is more useful for more highly absorbent surfaces in a broader frequency range.

Table III. Improvements of errors using $r_{\mathrm{fin,sq}}$ for BC1 in the proportionate room.

	$f_{\mathrm{lim}}/f_{\mathrm{sch}}$	$\overline{\Delta e}$	Δe_{max}
$BC1_{,-80}$	1.0	1.1	4.1
$BC1_{,-60}$	1.0	1.4	3.4
$BC1_{,-40}$	0.8	0.7	2.2
$BC1_{,-20}$	0.5	0.4	1.7
$BC1_{,0}$	0.5	0.3	1.5
$BC1_{,20}$	0.5	0.2	1.1
$BC1_{,40}$	0.2	0.1	0.7
$BC1_{,60}$	0.4	0.2	0.6
$BC1_{,80}$	1.5	1.7	2.7

Table IV. Improvements of errors using $r_{\mathrm{fin,sq}}$ for BC2 in the proportionate room.

	$f_{\mathrm{lim}}/f_{\mathrm{sch}}$	$\overline{\Delta e}$	Δe_{max}
$BC2_{,-60}$	1.4	2.2	5.0
$BC2_{,-40}$	1.4	1.2	3.4
$BC2_{,-20}$	1.1	0.7	2.4
$BC2_{,0}$	0.7	0.3	1.6
$BC2_{,20}$	0.7	0.2	0.9
$BC2_{,40}$	1.1	0.2	0.4
$BC2_{,60}$	2.2	0.6	0.9

Table V. Improvements of errors using $r_{\mathrm{fin,sq}}$ for BC3 in the proportionate room.

	$f_{\mathrm{lim}}/f_{\mathrm{sch}}$	$\overline{\Delta e}$	Δe_{max}
$BC3_{,-60}$	1.3	1.7	5.3
$BC3_{,-40}$	1.3	1.2	3.6
$BC3_{,-20}$	1.1	0.7	2.5
$BC3_{,0}$	1.1	0.4	1.6
$BC3_{,20}$	2.7	0.3	0.7
$BC3_{,40}$	2.7	0.4	0.6
$BC3_{,60}$	2.7	0.8	1.5

Table VI. Improvements of errors using $r_{\mathrm{fin,sq}}$ for BC4 in the proportionate room.

	$f_{\mathrm{lim}}/f_{\mathrm{sch}}$	$\overline{\Delta e}$	Δe_{max}
$BC4_{,-40}$	3.1	1.1	3.4
$BC4_{,-20}$	3.1	0.8	2.3
$BC4_{,0}$	3.1	0.6	1.4
$BC4_{,20}$	3.1	0.4	0.5
$BC4_{,40}$	3.1	0.5	0.6

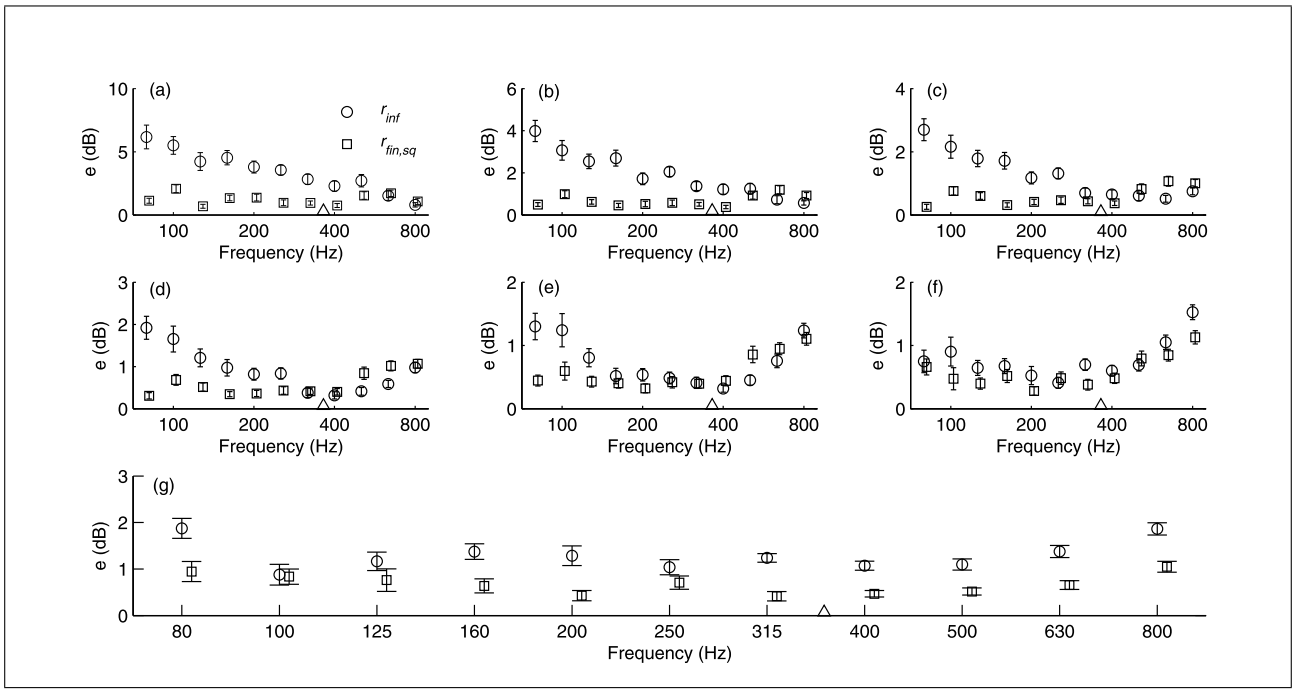


Figure 3. Errors averaged over the receiver positions as a function of frequency in the proportionate room for BC2. The error bars indicate 95% confidence intervals and Δ indicates the Schroeder frequency. (a) -60°; (b) -40°; (c) -20°; (d) 0°; (e) 20°; (f) 40°; (g) 60°.

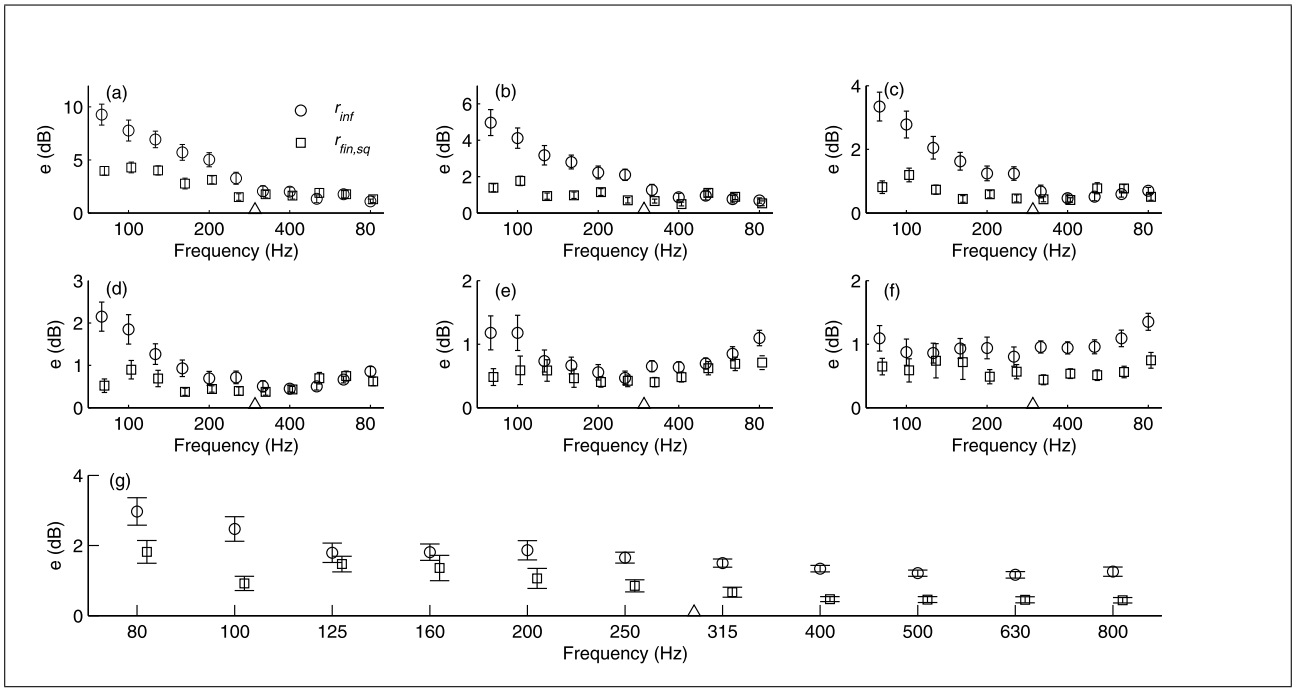


Figure 4. Errors averaged over the receiver positions as a function of frequency in the proportionate room for BC3. The error bars indicate 95% confidence intervals and Δ indicates the Schroeder frequency. (a) -60°; (b) -40°; (c) -20°; (d) 0°; (e) 20°; (f) 40°; (g) 60°.

Although only four cases are displayed in Figure 6, the simulation results with $r_{\mathrm{fin,Rindel}}$ are consistently less accurate than those with $r_{\mathrm{fin,sq}}$. For $\mathrm{BC1}_{,0}$ the difference between $r_{\mathrm{fin,Rindel}}$ and $r_{\mathrm{fin,sq}}$ is the smallest due to the largest value of the surface impedance in Figure 6a, since the reflection coefficient is heavily influenced by the ratio of the surface impedance to the radiation impedance by equation (4). For complex-valued surface impedances in Figures 6b and 6d, it is natural that the omission of the imaginary part using $\zeta_{\mathrm{rad,Rindel}}$ leads to inaccurate reflection coefficients. The results using r_{Thom} are not shown, because it leads to overly large errors for all the test cases. The additional error using r_{Thom} in comparison to the infinite panel theory is approximately 1–3 dB over the entire frequency range.

Two examples of the calculated transfer functions in Figures 7a and 7b illustrate how the suggested reflec-

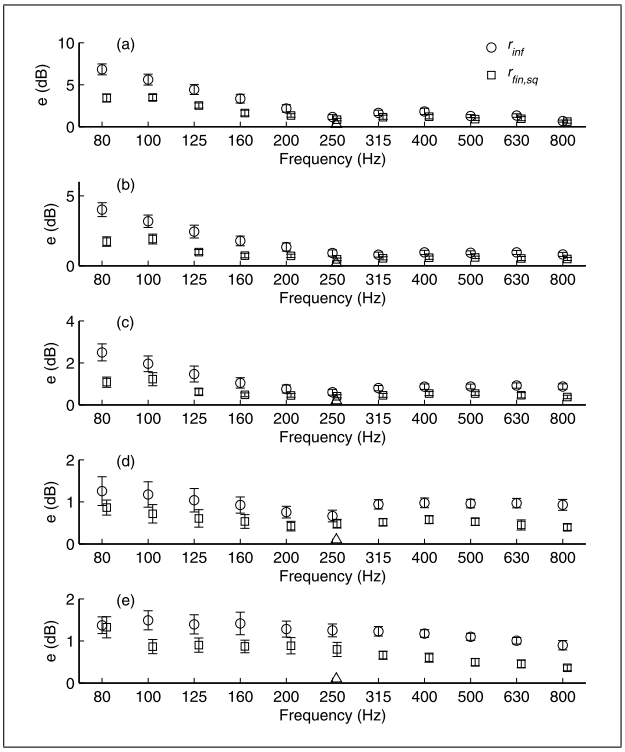


Figure 5. Errors averaged over the receiver positions as a function of frequency in the proportionate room for BC4. The error bars indicate 95% confidence intervals and Δ indicates the Schroeder frequency. (a) -40°; (b) -20°; (c) 0°; (d) 20°; (e) 40°.

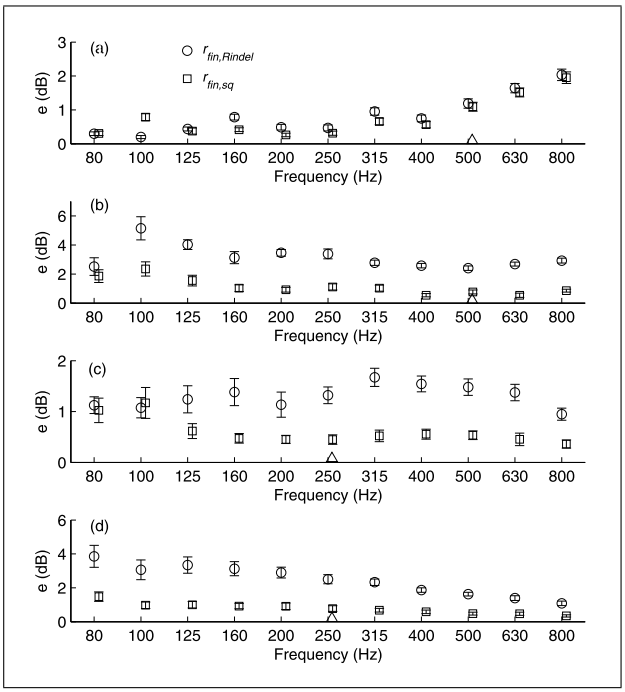


Figure 6. Errors averaged over the receiver positions as a function of frequency in the proportionate room. The error bars indicate 95% confidence intervals and Δ indicates the Schroeder frequency. (a) $BC1_{,0}$; (b) $BC1_{,80}$; (c) $BC4_{,0}$; (d) $BC4_{,40}$.

tion coefficient improves the transfer function calculations. Three PBTM simulations with $r_{\mathrm{inf,Thom}}$ and $r_{\mathrm{fin,sq}}$ are compared to the corresponding BEM simulation at a receiver (0.5, 0.4, 0.3): $BC1_{,0}$ in Figure 7a and $BC4_{,0}$ in Figure 7b. One can observe overly pronounced peaks and troughs using r_{Thom} in Figure 7a because of the overestimated reflection coefficient value, while the simulation with $r_{\mathrm{fin,sq}}$ leads to more correct peak and trough values than r_{inf}, particularly at low frequencies. Also for $BC4_{,0}$, the low frequency levels are predicted accurately by $r_{\mathrm{fin,sq}}$, whereas r_{inf} underestimates and r_{Thom} overestimates the true response. Some discontinuities found in the simulation with $r_{\mathrm{fin,sq}}$, e.g., at around 90 Hz in Figure 7b, are due to the fact that a limited number of reflection coefficients are calculated only at the center frequencies of the octave bands and used for calculating the transfer functions.

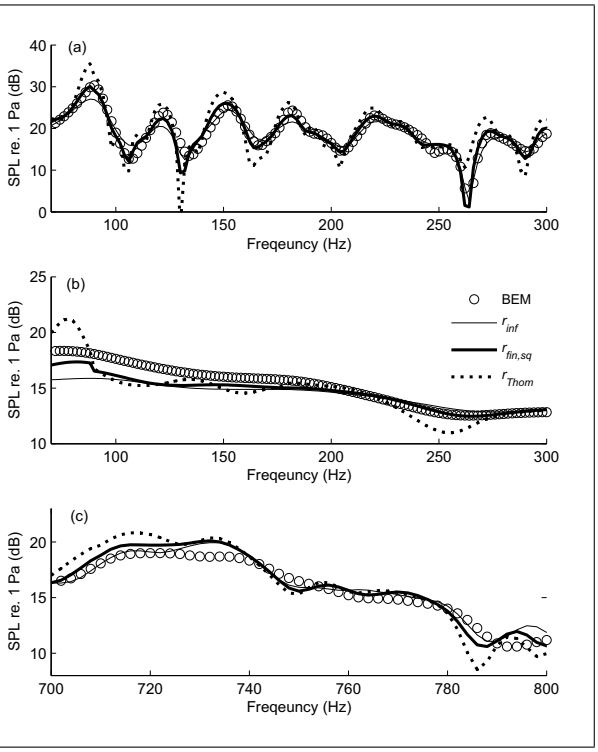


Figure 7. Simulated transfer functions at (0.5, 0.4, 0.3) in the proportionate room. (a) $BC1_{,0}$ at low frequencies; (b) $BC4_{,0}$ at low frequencies; (c) $BC1_{,0}$ at high frequencies.

However, the suggested reflection coefficients yield larger errors than r_{inf} at frequencies above f_{lim} for the low absorption cases of BC1 and BC2. Figure 7c compares transfer functions above the Schroeder frequency for BC1 at the same receiver as Figure 7a. The prediction with r_{inf} at high frequencies is slightly overestimated, and the prediction with $r_{\mathrm{fin,sq}}$ is slightly more overestimated than the infinite panel theory, since $r_{\mathrm{fin,sq}}$ is generally larger than r_{inf}. Since $r_{\mathrm{fin,sq}}$ converges to r_{inf} for sufficiently large panels at sufficiently high frequencies, it is expected that r_{inf} and $r_{\mathrm{fin,sq}}$ produce similar results. However, the proportionate room is too small with an averaged e value of 1.4, and therefore even at 800 Hz, the ke value is not sufficiently large for the finite-sized radiation impedance to converge to $1/\cos(\theta)$. Figure 8 compares r_{inf}, $r_{\mathrm{fin,sq}}$, and r_{Thom} for $BC1_{,0}$ at an incidence angle of 45°, which is

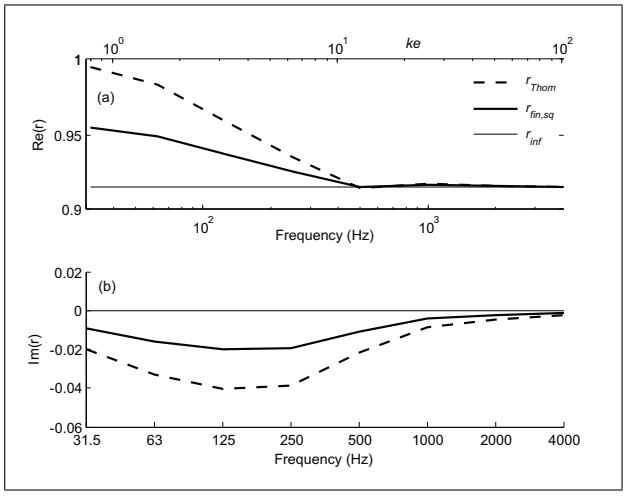


Figure 8. Reflection coefficients for $BC1_{,0}$. (a) Real part; (b) imaginary part.

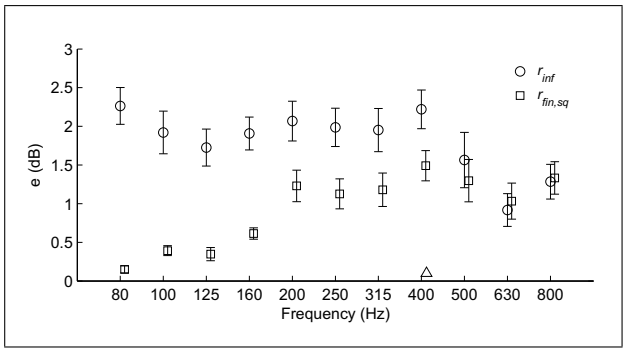


Figure 9. Errors averaged over the receiver positions as a function of frequency for NONU. The error bars indicate 95% confidence intervals and Δ indicates the Schroeder frequency.

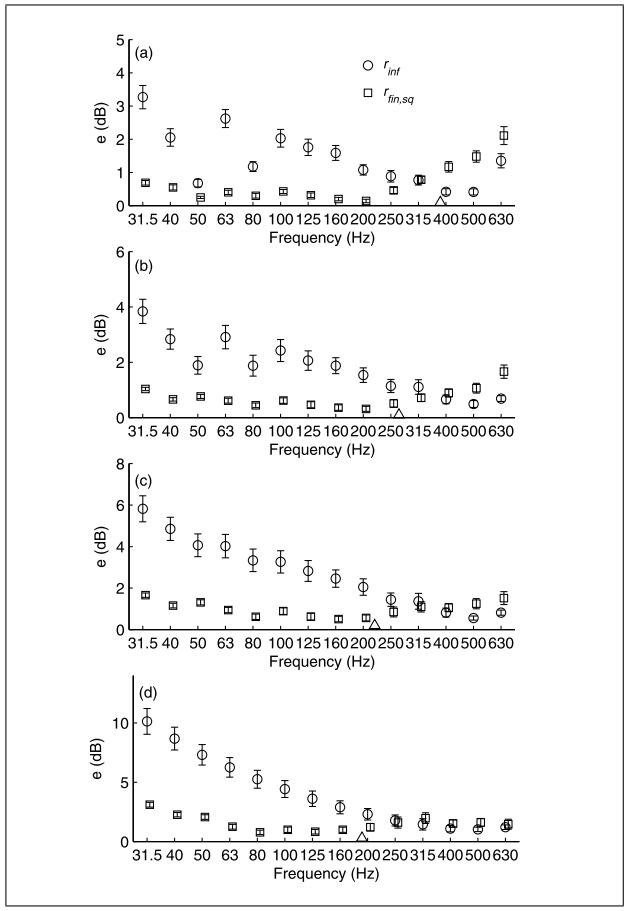


Figure 10. Errors averaged over the receiver positions as a function of frequency in the disproportionate room. The error bars indicate 95% confidence intervals and Δ indicates the Schroeder frequency. (a) $BC1_{,0}$; (b) $BC2_{,0}$; (c), $BC3_{,0}$; (d) $BC4_{,0}$.

likely to best represent the random incidence condition [20]. Larger discrepancies in the real part of the reflection coefficient are found up to 500 Hz, which corresponds to a ke value of 13. $r_{\mathrm{fin,sq}}$ is larger than r_{inf} at low frequencies, but finally converges to r_{inf} at around 2 kHz that corresponds to a ke value of around 50. Note the imaginary part of r_{inf} is always zero. One can notice slightly larger $r_{\mathrm{fin,sq}}$ than r_{inf} at around 1 kHz, which degraded the simulations for BC1 conditions above the Schroeder frequency. Note, however, that despite the increased errors at high frequencies, the averaged error over the entire frequency range is always lower with $r_{\mathrm{fin,sq}}$ for all the cases tested as shown in Tables III to VI.

4.2. Non-uniform absorption in the proportionate room

In Figure 9, the error for NONU is shown. NONU has a mean random incidence absorption coefficient of around 0.3, therefore one may expect a similar result to $BC1_{,0}$ and $BC2_{,0}$. However, the improvements are larger than for the uniform real-valued impedance boundary conditions; $\overline{\Delta e}$ is 1.1 dB and $\Delta e_{\max}$ is 2.1 dB. This is partly because the error with r_{inf} for NONU is larger than for $BC1_{,0}$; $\overline{e}$, the average error over the entire frequency range with r_{inf} for NONU is 1.8 dB, while $\overline{e}$ with r_{inf} for $BC1_{,0}$ is 1.0 dB. With $r_{\mathrm{fin,sq}}$, the error is reduced to 0.9 dB for NONU, but slightly decreased to 0.7 dB for $BC1_{,0}$, thus NONU and $BC1_{,0}$ having a similar absorption coefficient yield similar errors using $r_{\mathrm{fin,sq}}$.

4.3. Uniform absorption in the disproportionate room

The disproportionate room tends to produce larger errors than the proportionate room by using r_{inf} [3]. For the disproportionate room, only four real-valued surface impedances are compared between r_{inf} and $r_{\mathrm{fin,sq}}$. Again similar trends are found in Figure 10 and Table VII; as the absorption coefficient increases, the improvement becomes larger, and the limiting frequency ratio, $f_{\mathrm{lim}}/f_{\mathrm{Sch}}$, becomes higher.

In Figure 10, large low frequency improvements are noticeable. Particularly fluctuations in the frequency range from 31.5 Hz to 100 Hz with r_{inf} in Figure 10a disappear by use of $r_{\mathrm{fin,sq}}$. However, above 315 Hz, the suggested reflection coefficient yields larger errors than r_{inf}. Figures 10b–d and Table VII reveal that the improvements are substantial at the lowest frequencies in the disproportionate

Table VII. Improvements of errors using $r_{\text{fin,sq}}$ in the disproportionate room.

	$f_{\text{lim}}/f_{\text{sch}}$	$\overline{\Delta e}$	Δe_{max}
$BC1_{,0}$	0.7	0.9	2.6
$BC2_{,0}$	1.2	1.2	2.8
$BC3_{,0}$	1.5	1.9	4.2
$BC4_{,0}$	1.3	2.8	7.0

room. Compared to the proportionate room, the improvements are much larger; the maximum improvement for $BC4_{,0}$ is 7.0 dB for the disproportionate room, while it is just 1.4 dB for the same boundary condition in the proportionate room.

5. Discussions

The suggested reflection coefficient enhances the accuracy of the calculated transfer functions mainly at low frequencies. The improvement over the infinite panel theory becomes larger for the disproportionate rectangular room and non-uniformly distributed absorption case, which is a positive aspect in simulating actual rooms. For the same room geometry, larger improvements are found for more absorbing boundary conditions and larger negative phase shifts on reflection.

For acoustically hard surfaces, the first and second configuration mentioned in Chapter 2.1 become similar, and the idea of using the average radiation impedance of these two configurations would not be effective as shown in Figure 2, since all three configurations become relatively similar. Mathematically it is because of the ratio of the surface impedance to the radiation impedance (ζ/ζ_{rad}) being quite large whatever radiation impedance is used, making high surface impedance cases less dependent on the radiation impedance used. Therefore one finds the least improvement for BC1 using $r_{\text{fin,sq}}$, but improvement becomes larger for more acoustically absorbing surfaces, thus the best improvement is found for BC4.

It is also partly because the sphericity error is the most severe for BC4, as also pointed out by earlier studies [2, 3], and the suggested reflection coefficient seems to have a similar influence as the spherical-wave reflection coefficient. The spherical-wave reflection coefficient is known to enhance the prediction accuracy for small and long rooms at low frequencies and at grazing incidence [2, 21]. The spherical wave reflection coefficient is given by

$$r_s = r_p + (1 - r)F(w_n). \tag{9}$$

Here, $F(w_n)$, which is known as the boundary loss factor [21] or residual term caused by the sphericity of the wave, $F(w_n) = 1 + \mathrm{j}\sqrt{\pi} w_n \mathrm{e}^{-w_n^2} \mathrm{erfc}(-\mathrm{j}w_n)$, w_n is the numerical distance as $w_n = \sqrt{kd_n/2}(1+\mathrm{j})(\cos\theta + 1/\zeta)$ and d_n is the distance from the source to receiver. For higher frequencies, longer distance, and smaller surface impedances, w_n gets much larger than unity and $F(w_n)$ vanishes. Thus the spherical wave reflection coefficient becomes reduced to the plane wave reflection coefficient. However, at low frequencies the spherical wave reflection coefficient differs from plane wave reflection coefficient. The spherical wave reflection coefficient is larger due to the additional term in equation (9), which can explain why and how the use of $r_{\text{fin,sq}}$ that is larger than r_{inf} at low frequencies improves the simulations, as also seen in Figure 7.

Larger improvements are found for the complex-valued surface impedance boundary conditions. The larger the phase angle, the larger the imaginary part of the impedance. Then, it is not difficult to guess that once both surface impedance and radiation impedance are complex-valued, the imaginary part of the radiation impedance interact more with the imaginary part of the surface impedance as shown in equation (4), and consequently affecting the reflection coefficient to a larger degree. Therefore the radiation impedance of an infinitely large surface, being $1/\cos\theta$, leads to larger errors for complex-valued surface impedances, whereas complex-valued $\zeta_{\text{rad,fin}}$ produces smaller errors. The larger improvements for the complex-valued surface impedances are good indications that the suggested $\zeta_{\text{rad,fin}}$ is more correct than $1/\cos\theta$.

The negative phase angles of the surface impedance (or the negative reactance term) mean that sound is reflected from a plane situated at some distance behind the physical boundary, leading to positive time delays [22]. In other words, the acoustical volume of the room is larger than the physical volume, thus shifting the peaks toward low frequencies. In general, porous absorbers have negative phase angles [22], so the larger improvements with the suggested reflection coefficient for the negative phase angles are also a positive aspect for simulating actual rooms with porous absorbers installed.

The non-uniform absorption case is improved with $r_{\text{fin,sq}}$ more significantly than the similar uniform absorption cases, i.e., $BC1_{,0}$. For rooms with uniformly distributed absorption, the third configuration is always more similar to the infinite panel theory, that is the first configuration, than the second configuration in Figure 1, since at least the surrounding material has the same acoustic characteristic as the absorber of interest. However, for non-uniformly distributed absorption cases, it is not always the case, e.g., the four sides of the absorptive floor are connected to the reflective vertical walls having a large surface impedance of 38 in NONU setting in this study, thus this configuration becomes closer to the second configuration. Therefore $\zeta_{\text{rad,baffle}}$ plays a more crucial role in $\zeta_{\text{rad,fin}}$ in equation (4), thus enhancing the simulation accuracy more for NONU than for $BC1_{,0}$.

In most cases, $r_{\text{fin,sq}}$ outperforms $r_{\text{fin,Rindel}}$, which indicates that the imaginary part of the radiation impedance is important in calculating the reflection coefficients for finite surfaces, while the imaginary part was found to hardly change the transmission coefficient [13]. The use of $r_{\text{fin,sq}}$ leads to more accurate results for small surface impedances, since the reflection coefficient, which is defined as the combination of the surface impedance and the radiation impedance, $(\zeta - \zeta_{\text{rad}})/(\zeta + \zeta_{\text{rad}})$, is more heavily

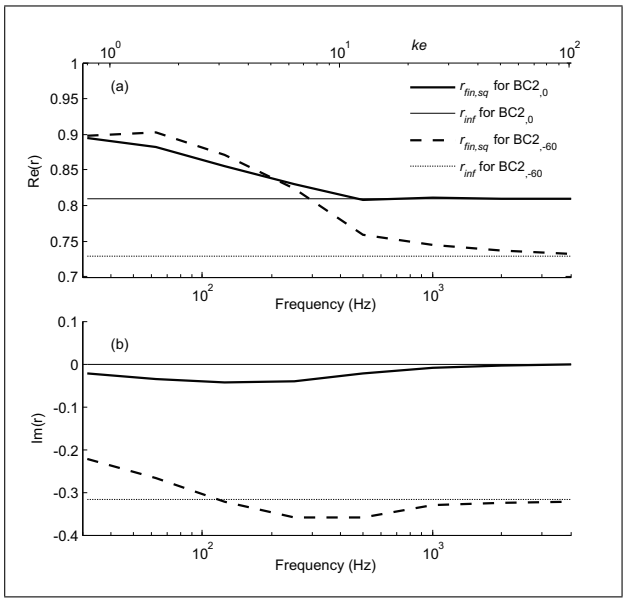


Figure 11. Reflection coefficients for $BC2_{,0}$ and $BC2_{,-60}$. (a) Real part; (b) imaginary part.

influenced by $\Im m(\zeta_{\mathrm{rad}})$ for small surface impedance values.

According to Figure 8, the suggested reflection coefficient significantly differs from the infinite-panel reflection coefficient up to a ke value of 13, which is quite consistent for real-valued impedance boundary conditions. However, for complex-valued surface impedances, the discrepancies are more pronounced as shown in Figure 11; the two reflection coefficients become similar at around 4 kHz, in other words, at a ke value of 100. Considering a cubic room of 1000 m^3, where e is 10 m, this value corresponds to 550 Hz, which is a fairly high frequency.

All in all, the suggested reflection coefficient for finite surfaces is concluded to be beneficial mainly for simulating low frequency behaviors of rectangular rooms. From the simulation examples investigated, one can conclude that the suggested reflection coefficient can be applied to proportionate rooms with averaged absorption coefficients beyond 0.6, non-uniformly distributed absorption cases with average absorption coefficients beyond 0.3, and disproportionate rooms with average absorption coefficients above 0.4, at least up to the Schroder frequency. For high frequency predictions well above the Schroder frequency and/or large rooms, it is also recommended to employ the infinite panel theory, unless the room is acoustically dead.

6. Future works

One point worth mentioning is that the suggested reflection coefficient is simply based on the arithmetic mean value of the radiation impedances of the first two configurations in Figure 1 for all frequencies. Since it has not been investigated whether or not the weighting factor of ½ for both $\zeta_{\mathrm{rad,fin}}$ and $1/\cos\theta$ is best, it is difficult to conclude what the optimum weighting factor is. Intuitively, the weighting factor for $\zeta_{\mathrm{rad,fin}}$ and $1/\cos\theta$ should depend on the frequency and the degree and distribution of absorption in the room, e.g., larger weighting factors for $1/\cos\theta$ would be more appropriate, as the frequency increases.

Although the suggested reflection coefficient improves the low frequency predictions, worsened high frequency responses for acoustically live rooms are drawbacks.
To overcome such weaknesses, a frequency-dependent weighting factor can also be incorporated to the suggested reflection coefficient. Once the limiting frequency, f_{lim}, is approximately estimated based on the results in this study, another new reflection coefficient adopting a frequency-dependent weighting factor can be suggested as

$$r_n = \begin{cases} r_{\mathrm{fin,sq}}(1-f_n) + r_{\mathrm{inf}}(f_n) & \text{for } f < f_{\mathrm{lim}}, \\ r_{\mathrm{inf}} & \text{for } f > f_{\mathrm{lim}}, \end{cases} \tag{10}$$

where f_n is the frequency ratio, f/f_{lim}. r_n surely improves the simulation accuracy, but f_{lim} varies with the geometry of the room and the distribution of absorption, thus it seems difficult to estimate f_{lim} correctly. Yet another rough approximation is to assume f_{lim} as f_{Sch}. In addition, various room shapes and non-uniform absorption cases can be further tested using the suggested reflection coefficient.

7. Conclusions

This study suggested a new reflection coefficient that improves low frequency room responses by considering the finite size of the boundary surfaces. The new reflection coefficient employs the arithmetic average value of the radiation impedance of an infinite panel and that of the finite-sized yet rigidly baffled panel, based on the fact that the sound pressure over the finite-sized boundary surface in a rectangular room would be in-between those over the infinitely extended surface and rigidly baffled finite surface. The suggested reflection coefficient improves predicted sound pressures at low frequencies for all tested uniform absorption cases, and it is most effective for highly absorptive surfaces and large negative phase shift on reflection. A larger improvement is found for a non-uniform absorption distribution than a uniformly distributed absorption having a similar absorption characteristic to the non-uniform setting. Larger improvements are found for a disproportionate room than a proportionate room. It is advised to use the suggested reflection coefficient based on the complex-valued radiation impedance by equation (6) or Table I, when simulating low frequency responses in small rectangular rooms.

References

[1] E. T. Paris: On the coefficient of sound-absorption measured by the reverberation method. Phil. Mag. **5** (1928) 489–497.

[2] Y. W. Lam: Issues for computer modelling of room acoustics in non-concert hall settings. Acoust. Sci. Tech. **26** (2005) 145–155.

[3] C.-H. Jeong: Absorption and impedance boundary conditions for phased geometrical acousitcs methods. J. Acoust. Soc. Am. **132** (2012) 2347–2358.

[4] ISO 354: Acoustics – Measurement of sound absorption in a reverberation room. 2003.

[5] S.-I. Thomasson: On the absorption coefficient. Acustica **44** (1980) 265–273.

[6] C.-H. Jeong: A correction of random incidence absorption coefficients for the angular distribution of acoustic energy under measurement conditions. J. Acoust. Soc. Am. **125** (2009) 2064–2071.

[7] C.-H. Jeong: Non-uniform sound intensity distributions when measuring absorption coefficients in reverberation chambers using a phased beam tracing. J. Acoust. Soc. Am. **127** (2010) 3560–3568.

[8] C.-H. Jeong, J.-G. Ih, J. H. Rindel: An approximate treatment of reflection coefficient in the phased beam tracing method for the simulation of enclosed sound fields at medium frequencies. Appl. Acoust. **69** (2008) 601–613.

[9] S. Ljunggren: Air-borne sound insulation of single walls at low frequencies: a discussion on the influence of boundary and mounting conditions. Build. Acoust. **8** (2001) 257–267.

[10] ASTM C423: Standard test method for sound absorption and sound absorption coefficients by the reverberation room method. 2009.

[11] S.-I. Thomasson: Theory and experiments on the sound absorption as function of the area. Report TRITA-TAK 8201, KTH, Stockholm, Sweden, 1982.

[12] J. H. Rindel: Modeling the angle-dependent pressure reflection factor. Appl. Acoust. **38** (1993) 223–234.

[13] J. Brunskog: The forced sound transmission of finite single leaf walls using a variational technique. J. Acoust. Soc. Am. **132** (2012) 1482–1493.

[14] M. Vorländer: Auralization: fundamentals of acoustics, modelling, simulation, algorithms and acoustic virtual reality. First edition. Springer-Verlag, Berlin, 2008.

[15] M. Hodgson, A. Wareing: Comparisons of predicted steady-state levels in rooms with extended- and local-reaction bounding surfaces. J. Sound Vib. **309** (2008) 167–177.

[16] B. Yousefzadeh, M. Hodgson: Energy- and wave-based beam-tracing prediction of room-acoustical parameters using different boundary conditions. J. Acoust. Soc. Am. **132** (2012) 1450–1461.

[17] C.-H. Jeong, J.-G. Ih: Effects of source and receiver locations in predicting room transfer functions by a phased beam tracing method. J. Acoust. Soc. Am. **131** (2012) 3864–3875.

[18] T. Lewers: A combined beam tracing and radiant exchange computer-model of room acoustics. Appl. Acoust. **38** (1993) 161–178.

[19] P. M. Morse, K. U. Ingard: Theoretical acoustics. McGraw-Hill, New York, 1968.

[20] C.-H. Jeong, J. Brunskog: The equivalent incidence angle for porous absorbers backed by a hard surface. J. Acoust. Soc. Am. (2013) in press.

[21] K. M. Li, K. K. Iu: Propagation of sound in long enclosures. J. Acoust. Soc. Am. **116** (2004) 2759–2770.

[22] J. H. Rindel: An impedance model for estimating the complex pressure reflection factor. Forum Acusticum 2011, CD-Rom, 2011.